THE ASTROPHYSICAL JOURNAL, 376:312–321, 1991 July 20

SMM/HXRBS OBSERVATIONS OF CYGNUS X-1 FROM 1986 DECEMBER TO 1988 APRIL

R. A. SCHWARTZ,[1,2] L. E. ORWIG,[1] B. R. DENNIS,[1] J. C. LING,[3] AND W. A. WHEATON[3]

Received 1990 September 28; accepted 1991 January 17

ABSTRACT

We report on 30 hard X-ray measurements of Cygnus X-1 made with a *Solar Maximum Mission* (*SMM*) Hard X-Ray Burst Spectrometer (HXRBS); 24 offset points from solar pointing were made to view Cygnus X-1 from 1986 December 22 through 1987 April 3, and six additional observations from 1988 January 28 through March 8. This resulted in a data set broad in synoptic coverage (6 months spread over ~1.5 yr) but of limited duration (60–70 minutes) for each data point. Ling et al. had previously identified three levels of the 50–300 keV flux from Cygnus X-1 during observations made with *HEAO 3* in 1979 and 1980. In order of increasing intensity they named these levels γ_1, γ_2, and γ_3. During the observations reported here, the hard X-ray intensity lay between the γ_2 and the γ_3 levels with a range of fluctuations about the average intensity level similar to the range seen by both *HEAO 1* and *HEAO 3*. There was a single observation on 1987 February 24 where the flux exceeded the γ_3 level, although the flux was close to its average level for 1987 during both the preceding and following observations on 1987 February 19 and March 3. For both the observations in 1987 and 1988, the shape of the photon spectrum was found to be closest to that reported by Ling et al. during the time of the γ_3 level emission, although the spectral shapes reported for the γ_2 and γ_1 levels could not be ruled out.

Subject headings: stars: individual (Cygnus X-1) — X-rays: binaries — X-rays: spectra

1. INTRODUCTION

Cygnus X-1 is one of the most studied objects in the X-ray/gamma-ray sky because it is bright, variable on many time scales, spectrally variable, and thought to be powered by mass accretion from a ~30 $M_\odot$ blue supergiant onto a 10–15 $M_\odot$ compact object that is generally believed to be a black hole. From early satellite and balloon measurements (Tananbaum et al. 1972; Holt et al. 1976; Matteson et al. 1976) two anti-correlated soft (1–10 keV) and hard (~20–200 keV) X-ray states of the emission from Cygnus X-1 were identified (Tananbaum et al. 1972; Coe, Engel, & Quenby 1976; Dolan et al. 1977; Ogawara et al. 1982), known as the soft X-ray low and high states. The "low" state has been the more common and is characterized by a lower soft X-ray intensity but a harder spectrum, resulting in increased hard X-ray flux as compared to the "high" state.

Observations of the hard X-ray intensity of Cygnus X-1 have been sporadic. A 20 yr record (1965–1985) of the integral flux in the 45–140 keV range was recently compiled by Ling et al. (1987a). Measurements with the high-resolution gamma-ray spectrometer on the *HEAO 3* spacecraft in 1979 and 1980 (Ling et al. 1983; Ling et al. 1987b) have shown three levels of hard X-ray (~50–300 keV) emission during the soft X-ray low state measured with the *Ariel 5* All Sky X-ray Monitor (3–6 keV, see Ling et al. 1983) and the Hakucho instrument (1–12 keV; see Oda 1980a, b; Ogawara et al. 1982). The three levels, in order of increasing intensity, are identified as γ_1, γ_2, and γ_3 (Ling et al. 1987b). Ling et al. (1987a) show that most observations since 1971 have found the hard X-ray flux to be close to the γ_2 level. The spectrum during the γ_1 or so-called super-low level is flatter than those during the times of the γ_2 or γ_3 levels, crosses over to become more intense above ~400 keV, and has a strong component of gamma-ray emission near ~1 MeV (Ling et al. 1987b). The source has been observed to make transitions among these levels on time scales of days to weeks, perhaps controlled by properties associated with the accretion stream from the star to the compact object. The MeV emission observed in the γ_1 spectrum has been interpreted as strong evidence for theoretically predicted Comptonized thermal bremstrahlung emission produced in a superheated (~4×10^9 K) pair-dominated plasma in the innermost region of the accretion disk (Liang & Dermer 1988). There is also marginal evidence of narrow line emission at 511 keV in the γ_1 spectrum of Cygnus X-1 (Ling & Wheaton 1989a). Because of the strong similarity in both spectral and temporal behavior to that of the X-ray and gamma-ray source in the Galactic center region, Lingenfelter & Ramaty (1989) and Ling & Wheaton (1989b) have suggested that the Galactic center may also harbor a stellar-size black hole, and that the combination of the 1 MeV excess emission and a narrow 511 keV electron-positron annihilation line could be a unique gamma-ray feature for characterizing black holes.

At the time of these observations, HXRBS was the only instrument capable of continuing the long-term synoptic record of the hard X-ray emission from Cygnus X-1. Thus, we sought to establish the current flux level, map out any transitions, and measure possible differences in spectral shape between flux levels. Since both the *SMM* spacecraft and the HXRBS detector were designed for solar-pointed observing, neither was ideal for cosmic observations, and considerable effort had to be expended to obtain the observations and extract the spectrum and time history. The observations required that the HXRBS viewing axis, and with it the entire *SMM* spacecraft, be moved from its normal orientation toward the Sun to a point nearer to Cygnus X-1.

From 1986 December 22 through 1987 April 3, 24 observations of the hard X-ray spectrum of the black hole candidate

[1] Laboratory for Astronomy and Solar Physics, [Mail Code 602.6 (RAS); 682.2 (LEO & BRD)], NASA Goddard Space Flight Center, Greenbelt, MD 20771.

[2] Also ST Systems Corporation, Lanham, MD.

[3] Jet Propulsion Laboratory, California Institute of Technology, Mail Code 169-327, Pasadena, CA 91109.

TABLE 1

SUMMARY OF OFFPOINTS TO CYGNUS X-1

Offpoint (1)	Date (2)	Start Time (UT) (3)	Offpoint Duration (hr) (4)	Binary Phase (5)	Angle from Sun (6)	Angle from Cygnus (7)	Direction of Offpoint R.A. (8)	Direction of Offpoint Decl. (9)	Fractional Area (10)
1	12/22/86	0716:59	1.5917	0.21	40°	24°.87	287°.03	12°.98	0.316
2	12/24/86	0625:00	1.5666	0.56	40	24.00	288.16	13.44	0.339
3	12/29/86	0415:29	1.5834	0.46	40	21.95	290.82	14.64	0.395
4	01/07/87	1601:01	1.6080	0.15	40	18.57	295.12	17.01	0.489
5	01/09/87	1643:58	1.5920	0.51	40	17.92	296.20	17.48	0.507
6	01/11/87	1552:01	1.5910	0.87	40	17.65	296.60	17.70	0.514
7	01/17/87	1628:58	1.5920	0.94	40	15.97	299.20	19.20	0.562
8	01/20/87	1515:00	1.5750	0.47	40	15.38	300.24	19.80	0.578
9	01/26/87	1240:01	1.5750	0.50	40	14.57	302.20	20.80	0.601
10	01/30/87	1055:01	1.5910	0.22	40	14.29	303.40	21.30	0.609
11	02/01/87	1001:58	1.5920	0.57	40	14.29	304.06	21.46	0.609
12	02/08/87	0700:00	1.5917	0.78	40	14.45	306.30	22.01	0.605
13	02/13/87	0315:00	1.5917	0.67	40	14.91	307.90	22.20	0.592
14	02/17/87	0131:00	1.5916	0.34	40	15.50	309.40	22.32	0.575
15	02/20/87	0012:00	1.5917	0.88	40	16.11	310.70	22.38	0.558
16	02/24/87	2201:58	1.5750	0.77	40	17.17	312.70	22.45	0.528
17	03/03/87	1740:01	1.3750	0.98	50	9.26	308.00	29.35	0.750
18	03/05/87	1649:01	1.3830	0.33	50	9.96	308.90	29.20	0.731
19	03/10/87	1440:01	1.3750	0.18	50	12.10	311.70	28.90	0.671
20	03/13/87	1324:28	1.3340	0.72	50	13.03	312.90	28.80	0.645
21	03/23/87	0724:00	1.3750	0.46	50	17.27	318.50	28.90	0.525
22	03/27/87	0604:00	1.0000	0.17	60	9.26	310.20	32.60	0.750
23	03/30/87	0445:00	1.0167	0.71	60	10.71	312.00	32.60	0.710
24	04/03/87	0301:59	1.0000	0.42	60	12.59	314.40	32.80	0.657
25	01/28/88	1331:58	1.3170	0.04	45	9.49	301.59	25.85	0.744
26	02/18/88	0346:58	1.2970	0.75	45	10.65	306.63	26.46	0.711
27	02/23/88	2325:01	1.2830	0.77	45	11.72	308.36	26.27	0.681
28	03/01/88	2007:01	1.3160	0.98	45	13.67	311.27	25.99	0.627
29	03/03/88	1910:58	1.3340	0.34	45	14.31	312.20	25.93	0.608
30	03/08/88	1518:00	1.3330	0.23	45	16.08	314.73	25.85	0.559

Cygnus X-1 were made with the Hard X-Ray Burst Spectrometer (HXRBS) on the *Solar Maximum Mission* (*SMM*). Six additional observations were made from 1988 January 28 through March 8. These were the first *SMM* offpoints conducted for HXRBS observations, and the operational techniques and data analysis procedures were developed as the observations were being made. Table 1 shows the dates of all 30 observations together with various information about the offpoints from solar viewing. This paper describes the source-flux extraction technique and places limits on the systematic errors. We show that the average intensity of the flux from Cygnus X-1 lay between the more common γ_2 and more intense γ_3 levels; that the shape of the spectrum was most consistent with that found for the γ_3 level by Ling et al. (1987b); and that one observation on 1987 February 24 revealed an intensity greater than 3 σ above the γ_3 level. For the remainder of the observations, the flux showed a range of statistically significant fluctuations corresponding to $\sim$25% of the average value, a spread consistent with that reported by Nolan & Matteson (1983) and by Ling et al. (1983; 1987b) from the *HEAO 1* and *HEAO 3* data, respectively. No evidence for emission at the γ_1 level was found.

2. INSTRUMENTATION AND OBSERVATIONS

The HXRBS detector is a disk-shaped CsI(Na) scintillator crystal placed in a cylindrical cavity cut in a second large CsI(Na) crystal used as an active anticoincidence shield (Orwig et al. 1980). The central crystal is 0.635 cm thick, has an area of 71 cm^2, and is viewed from the rear by four 1″ RCA C31016f13 photomultiplier tubes (PMTs). The walls of the shield are 3.2 cm thick and define an $\sim$40° full width at half-maximum (FWHM) field of view (FOV). Central crystal events from $\sim$30–500 keV with no coincident pulses in the shield are accumulated into 15 energy channels. The number in each channel is read out every 128 ms along with the instrument live time. Typical count rates in the full energy range run from $\sim$35 s^{-1} for background to over 10^5 s^{-1} during the strongest solar flares. The pulse-height spectrum is calibrated in flight by the detection of 59.6 keV X-rays emitted by an Am^{241} radioactive source embedded in a plastic scintillator button located in the detector FOV near the top of the anticoincidence shield. These calibration spectra are composed of events coincident with 5 MeV alpha particle signals detected with a PMT from the scintillator button.

During the period of the Cygnus observations, the *SMM* spacecraft was in a nearly circular orbit at an altitude of $\sim$480 km, with an orbital period of $\sim$96 minutes and an inclination of 28°.5. The 3 axis–stabilized spacecraft was normally pointed at the Sun such that the HXRBS FOV was centered on the solar disk. Concerns for spacecraft safety related to maintaining power from the solar cells precluded pointing away from the Sun at angles of more than 60° (45° in 1988). Thus, since Cygnus X-1 is located 56° off the ecliptic plane, it was only possible to offset point to bring it into the HXRBS FOV during a four month period each year, resulting in observa-

tions being made from 1986 December 22 through 1987 April 3 and from 1988 January 28 through March 8.

The 30 Cygnus offpoints are summarized in Table 1. The date and time in columns (2) and (3) are for the beginning of the offpoint pitch maneuver, and the duration listed covers the whole time away from solar pointing. The Cygnus binary phase, given in column (5), is measured from superior conjunction using the parameters of Ninkov, Walker, & Yang (1987). The angle from the detector axis to the Sun is given in column (6) and to Cygnus X-1 in column (7). The right ascension and declination of the offpoint direction are in columns (8) and (9). The fractional area given in column (10) is the fraction of the 71 cm^2 area of the central detector exposed to Cygnus X-1 during the offpoint (FAREA—see eq. [1] below).

The offpoints were accomplished in 10–15 minutes by a spacecraft roll about the normal look-axis followed by two or three pitch maneuvers. The spacecraft maintained the final attitude to within a few arcseconds through the ~30–70 minutes of the source observation. The return to solar pointing was accomplished by means of more pitch and roll maneuvers. It is important to note that for all the Cygnus observations, the roll angle was chosen such that the offpoint could be achieved by rotating the spacecraft about its pitch axis. Thus, the projection of the vector to the source onto the plane of the detector disk was always along the same azimuth. This is important, as shown below, since it meant that the source illuminated the same side of the central crystal for all the observations, and any differences in the PMT gains did not result in apparent variations in source intensity. The total angle from the Sun was never sufficient to place the source directly at the center of the FOV; the angle between Cygnus X-1 and the detector axis ranged from 9° to 25° (see the angles from the Sun and from Cygnus X-1 listed in Table 1).

3. DATA ANALYSIS

Accurately measuring the spectrum of a strong cosmic source with HXRBS is simple in concept but operationally more difficult. The increased detector count rate from the source during the offpoint can be determined, in principle, by subtracting the off-source (normally solar-pointing) background from the on-source rate. The source flux is then obtained by dividing this difference by the detector area presented to the source at that angle. However, the off-source solar-pointing count rate varies because of many effects such as Earth albedo, diffuse and discrete cosmic sources in the FOV, magnetospheric events, solar flares, orbital radiation dose history, the local energetic particle distribution, and nuclear reactors on other spacecraft. Ideally, the systematic error due to such background variations would be minimized by averaging over a large set of observations, each obtained using some technique for rapidly modulating the source flux detected by the instrument. This was not possible in our case since each HXRBS observation was made as a single on-off measurement. Thus, it was necessary to model the background variations as a function of other independent components so that the background rate could be estimated during the on-source period.

A typical observation during a ~5 hr period on 1987 March 5 is shown in Figure 1 together with the predicted components of the count rate as a function of time. The HXRBS count rate, summed over all 15 energy channels (corresponding to ~30–500 keV) in 65.536 s bins, shown as the histogram versus time in Figure 1*a*. This rate varies from 26 to 55 counts s^{-1} over the three orbits shown from 1440 to 1925 UT. Initially, it rises from ~26 to ~40 counts s^{-1} while the spacecraft is moving from night to day. This rise results from the fact that the sky background [see curve 1(c)], composed primarily of the diffuse cosmic X-ray component, is brighter than the atmosphere when integrated over the HXRBS energy range. The peaks at 1510, 1610, and 1740 UT occur as the spacecraft moves to higher geomagnetic latitudes, where the energetic cosmic-ray particle distributions are more intense because of the lower cutoff rigidity. The sharper peak at 1610 UT is probably due to a magnetospheric effect at high latitude. The offpoint toward Cygnus X-1 stars at 1650 UT [see curve 1(b)], but the rise due to the source appears to blend smoothly with the trend in the rate preceding the offpoint. The sudden changes in the rate at 1715 and 1750 UT mark the beginning and ending of the source occulation by the Earth [see curve 1(b)]. The ~18 minute data gap around 1900 UT occurs as the HXRBS high voltages are turned off for passage through the South Atlantic Anomaly (SAA).

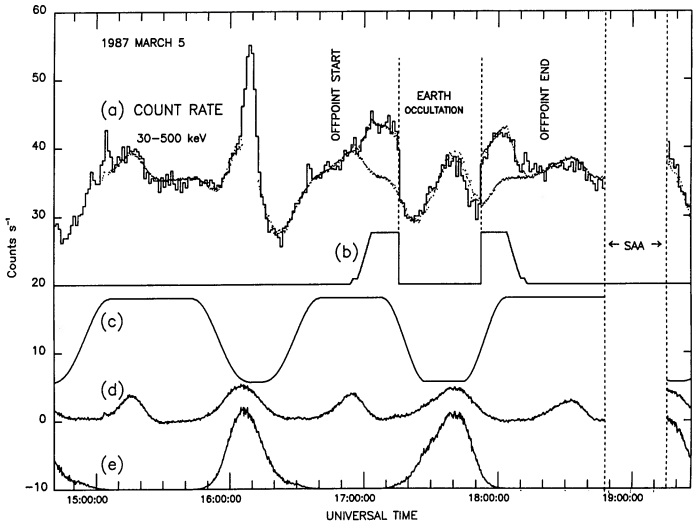

FIG. 1.—Typical observation of Cygus X-1 showing the measured HXRBS rates during a 3 orbit period that includes the offpoint on 1987 March 5 and the predicted rates from the background and source model discussed in the text (eq. [1]). Histogram (a) shows the measured HXRBS count rate summed over all 15 channels corresponding to an energy-loss range from 30 to 500 keV. According to the model, the predicted rate, shown as the dotted line, is made up of five components, a constant rate plus the four variable rates shown as curves (b)–(e). For this observation the constant term (A in eq. [1]) was 35.2 counts s^{-1}. The source component, $E \times$ FAREA, is plotted as curve (b) with an offset of +20 counts s^{-1} and a source flux, E, of 10.3 counts s^{-1}. Curve (c), offset by +18 counts s^{-1}, shows the term $C \times$ FFE with $C = -12.3$ counts s^{-1}. This component reflects the excess brightness of the diffuse sky X-ray background over the Earth's atmosphere. Curve (d) shows the component $B \times$ (ULR-ULR_{min}), with $B = 0.004$ and $ULR_{min} = 525$ counts s^{-1}. ULR is a measure of the energetic particle flux incident on the detector and is dependent on the cutoff rigidity. Curve (e) shows the term $D \times$ (ULR-ULR_{min}) $\times$ FFE offset by −10 counts s^{-1} with $D = 0.0087$. This component corrects for atmospheric brightening at higher latitudes where the geomagnetic cutoff rigidity is lower and the cosmic ray flux is higher. The sum of the model components is plotted as the dotted line through the histogram (a) with four dots for each histogram bin, as the actual time bins used in the fit were 16.384 s long. Predicted background during the offpoint is shown as the lower dotted line.

3.1. *The Parametric Background Model*

Although the background count rate is highly variable as shown in Figure 1*a*, a simplified model has been found to adequately fit most of the more gradual fluctuations. The

model is an outgrowth of an approach used by Wheaton et al. (1990) for the *HEAO 3* data analysis wherein one component of the background variation was found to be proportional to changes in their detector's upper level discriminator rate. Our background model includes this component and also models the difference in brightness between the atmosphere and the diffuse sky background as the Earth displaces the sky in the HXRBS FOV. In our model, the least-squares fit to the measured count rate, R_i, in time bin i is obtained for each of the 15 energy bins by calculating the free parameters—A, B, C, D, and E—which minimize the quantity $\Sigma_i(R_i - F_i)^2$, where F_i, the count rate predicted by the model, is given by the following expression:

$$F_i = A + B \times (\mathrm{ULR}_i\text{-}\mathrm{ULR}_{\min}) + C \times \mathrm{FFE}_i + D \times (\mathrm{ULR}_i\text{-}\mathrm{ULR}_{\min}) \times \mathrm{FFE}_i + E \times \mathrm{FAREA}_i . \quad (1)$$

The Upper Level Discriminator Rate (ULR) measures energy-loss events above ~ 500 keV in the central detector crystal, and $\mathrm{ULR}_{\min}$ was arbitrarily chosen to be 525 counts s^{-1}. The ULR provides an estimate of the isotropic integral energetic particle flux at the spacecraft. $B \times (\mathrm{ULR}_i\text{-}\mathrm{ULR}_{\min})$ is plotted as curve (d) in Figure 1. This component has two broad maxima during each orbit as the spacecraft moved between $\pm 28^\circ.5$ latitude. The fraction of the FOV filled by the Earth (FFE) varied from 1 to 0 as the spacecraft moved from night to day. The component proportional to FFE ($C \times \mathrm{FFE}_i$) models the difference between the brightness of the diffuse sky background and the Earth albedo flux; it is shown as curve (c) in Figure 1. $D \times (\mathrm{ULR}_i\text{-}\mathrm{ULR}_{\min}) \times \mathrm{FFE}_i$, shown as curve (e) in Figure 1, is included to allow for the increased brightness of the atmosphere at high latitude as indicated by high values of ULR and modified by the fraction of the FOV filled by the Earth. Finally, curve (b) maps the source component, $E \times \mathrm{FAREA}_i$, where E is the source flux and FAREA is the fraction of the detector area open to the source flux unblocked by the collimator or the Earth. This component was zero until the offpoint maneuvers moved the detector axis to within 40° of the source direction. The detector pointed to the offpoint direction, in this case $9^\circ.96$ from Cygnus X-1 (see Table 1), from ~ 1703 UT until 1804 UT, so FAREA remained constant except for the 35 minute interval when the source was occulted by the Earth.

3.2. *Parametric Fits to the Observations*

In our analysis procedure for each offpoint, the best-fit values of the five free parameters in equation (1) and their uncertainties were computed independently for each of the 15 energy channels. The values of the source flux, parameter E, for each energy bin were then used to obtain a photon spectrum of the source for each observation as discussed below. For the purpose of constructing Figure 1, we summed the best-fit values of the parameters over all 15 channels, and these values are given in Table 2 with their uncertainties.

TABLE 2

FIT PARAMETERS SUMMED OVER ALL 15 CHANNELS FOR THE SOURCE-PLUS-BACKGROUND MODEL[a]

Parameter (1)	Julian Day (−2,440,000) (2)	A (counts s^{-1}) (3)	σA (counts s^{-1}) (4)	B ($\times 10^{-4}$) (5)	σB ($\times 10^{-4}$) (6)	C (counts s^{-1}) (7)	σC (counts s^{-1}) (8)	D (10^{-4}) (9)	σD (10^{-4}) (10)	E (counts s^{-1}) (11)	σE (counts s^{-1}) (12)	Flux 45–140 keV $\left(\frac{\text{photons}}{\text{cm}^2\ \text{s}}\right)$ (13)	$\frac{\sigma(\text{Flux})}{\text{Flux}}$ (14)
1	6786.80	36.07	0.35	46	3.6	−10.99	0.61	62	4.8	12.42	0.87	0.153	0.238
2	6788.77	37.23	0.35	31	3.6	−12.30	0.65	83	4.9	9.79	0.88	0.130	0.284
3	6793.68	38.02	0.50	36	3.1	−13.05	0.76	68	4.6	7.39	1.26	0.089	0.354
4	6803.17	37.43	0.33	2[b]	19.0	−13.99	1.48	120	21.0	11.22	0.61	0.151	0.171
5	6805.20	35.50	0.38	33	6.5	−12.45	0.85	84	8.1	13.40	0.75	0.169	0.143
6	6807.16	35.82	0.43	11	6.6	−12.48	0.87	100	7.9	15.00	0.86	0.193	0.126
7	6813.19	36.24	0.31	35	3.8	−13.15	0.81	86	5.8	12.01	0.55	0.154	0.141
8	6816.14	35.65	0.39	54	3.7	−13.35	0.77	80	5.6	12.16	0.60	0.163	0.142
9	6822.03	36.74	0.36	64	3.8	−11.99	0.68	38	6.0	11.16	0.51	0.137	0.141
10	6825.95	36.36	0.21	46	2.8	−11.66	0.71	76	8.7	13.37	0.33	0.169	0.114
11	6827.92	35.77	0.18	51	2.7	−11.30	0.49	72	4.8	13.21	0.30	0.167	0.039
12	6834.79	36.01	0.12	46	2.6	−11.48	0.49	71	4.4	10.68	0.23	0.136	0.044
13	6839.64	35.70	0.10	32	1.9	−12.24	0.39	93	3.3	12.98	0.23	0.164	0.037
14	6843.56	35.00	0.11	39	1.8	−11.60	0.49	81	4.8	11.81	0.26	0.146	0.043
15	6846.51	34.75	0.11	39	1.8	−12.06	0.57	90	6.0	14.11	0.28	0.171	0.037
16	6851.42	33.95	0.09	44	1.7	−11.72	0.51	92	4.8	16.22	0.27	0.204	0.033
17	6858.24	35.30	0.10	32	2.2	−12.01	0.50	91	3.9	11.96	0.22	0.148	0.034
18	6860.20	35.21	0.11	40	2.4	−12.26	0.50	87	4.0	10.34	0.24	0.130	0.041
19	6865.11	35.65	0.12	47	2.1	−11.78	0.38	75	3.4	11.58	0.27	0.146	0.040
20	6868.06	35.58	0.11	54	2.2	−11.29	0.37	59	3.6	13.92	0.28	0.173	0.035
21	6877.81	35.50	0.11	45	2.3	−11.16	0.38	78	3.6	11.86	0.36	0.153	0.051
22	6881.75	35.44	0.11	45	2.5	−11.54	0.51	82	4.3	11.44	0.29	0.147	0.039
23	6884.70	35.40	0.10	40	2.4	−11.27	0.48	81	4.2	13.35	0.27	0.169	0.033
24	6888.63	34.58	0.09	38	2.1	−11.55	0.46	88	4.4	11.29	0.33	0.144	0.044
25	7189.06	34.91	0.10	49	2.1	−11.63	0.38	62	3.9	11.69	0.24	0.144	0.035
26	7209.66	33.97	0.10	40	2.2	−12.21	0.46	96	4.1	9.17	0.22	0.117	0.046
27	7215.48	33.17	0.08	40	1.8	−12.66	0.63	130	7.7	12.18	0.25	0.152	0.037
28	7222.34	32.96	0.08	39	2.1	−11.61	0.42	89	4.2	10.91	0.30	0.133	0.046
29	7224.30	32.83	0.08	37	2.5	−11.04	0.45	84	4.3	11.96	0.32	0.154	0.044
30	7229.14	33.24	0.10	39	3.2	−11.59	0.50	88	4.6	9.69	0.31	0.118	0.057

[a] See eq. (1).

[b] The uncertainties in B and D are large and highly correlated because the presence of the Galactic center sources rendered so much of the potential background time useless during observation #4.

How well the parametric fit of equation (1) agrees with the observation can be seen from the dotted line which follows the count rate histogram in Figure 1. During the offpoint observation, the lower dotted line indicates the predicted background rate with the source excluded. Any point, such as the peak at 1610 UT, was excluded from the fit if it was more than three standard deviations plus 2 counts s^{-1} from a preliminary fit. The two data bins adjacent to the occultation transition were also excluded to avoid the need to consider the effects of partial attenuation by the Earth's atmosphere and to relax the constraints on reconstructing the spacecraft ephemeris. The gradual peaks and valleys in the count rate are reproduced by the fit as is the transition from background to offpoint at 1655 UT. Most of the deviation of the fit from the model is consistent with the statistical uncertainties of ~ 0.8 counts s^{-1} in the measured count rate in each 65.536 s histogram bin, but there are a few short intervals, for example, 1745–1750 UT, where the fit appears to have a systematic deviation of 1 or 2 counts s^{-1} from the observations.

Our best results are obtained from data sets like that in Figure 1. Data covering almost three orbits roughly centered on the offpoint period were used for each observation. The effects of radioactive decay after SAA passage were minimized by doing the offpoints immediately prior to the first passage through the SAA on each day of the observations. Some data after the first SAA passage were used, but only if the first pass missed the bulk of the energetic ions responsible for the activation of the detector.

The first 10 Cygnus offpoints were somewhat different from the later offpoints, like the 1987 March 5 observation shown in Figure 1, because of the contamination by the hard X-ray flux from the Galactic center region during the solar-pointing background. Eliminating that portion of the data where the Galactic center was in the HXRBS FOV, that is, less than 40° from the Sun, left only the single Earth occultation to provide the modulation of the flux from Cygnus X-1; that is, we could not use the solar-pointing data in the determination of the free parameters of the model.

For all of the observations, Cygnus X-3, $\sim 9°$ from Cygnus X-1, was present in the FOV during the offpoints. However, it nearly always was at a greater angle to the center of the FOV than Cygnus X-1 and has less than 5% of the flux above 40 keV (Levine et al. 1984). Thus, we have assumed that all of the rate increase reflected in the source free parameter, E, is caused by Cygnus X-1.

3.3. *Spectral Deconvolution*

Once we derived the 15 channel count rate spectrum of the source for each observation, that is, the 15 values of the free parameter E, we had to take the instrument response function into account to determine the source photon spectrum using the deconvolution technique described by Batchelor (1984). While the response function can be thought of as a matrix which gives the probability of an input photon of energy ϵ being counted in channel j, the problem of explicitly inverting this matrix can be avoided if the input spectral shape is known or assumed, for example, power-law, exponential, thermal bremsstrahlung, Comptonized thermal, etc. Then, for a given shape, the response function can be used to calculate 15 numbers, called conversion factors, which are the ratio of the expected count rate in each channel to the photon flux at the midpoint energy of that channel. Many sets of such conversion factors have been calculated and stored in computer files for a wide range of spectral shapes for our spectral deconvolution routine. To begin the deconvolution procedure, a spectral shape is chosen by selecting both the specific model function, for example, power-law, and initial values of its free parameters. Then the corresponding conversion factors are used to deconvolve the measured count rate spectrum into a photon number spectrum. A least-squares fit of the same spectral form is then made to this photon number spectrum to determine refined free parameters, and these are used to select new conversion factors. The measured spectrum is then deconvolved a second time using these new conversion factors, and the process is repeated until there is an insignificant change in the free parameters from one interaction to the next. The results of this exercise are shown in Figure 2 where the assumed thermal bremsstrahlung spectrum for Cygnus X-1 on 1987 March 5 is shown as the smooth curve and the deconvolved photon number spectrum is shown as the data points. We have excluded the lowest of the 15 HXRBS channels from these spectral fits because of the uncertainty in the energy of the lower edge of this channel that is set by a discriminator independent of the other channel edges.

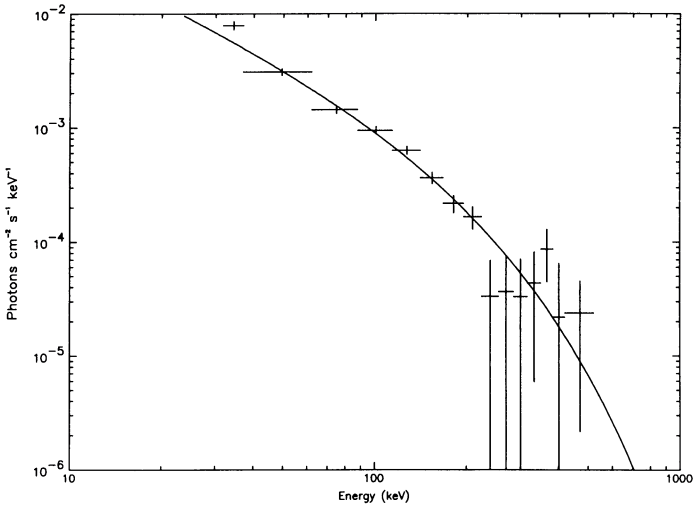

FIG. 2.—Deconvolved photon number spectrum for the 1987 March 5 observation of Cygnus X-1. Error bars represent $\pm 1\ \sigma$ uncertainties that are made up of the statistical uncertainty and a systematic uncertainty equal to 5% of the conversion factors designed to reflect the uncertainties in the detector model. Horizontal bars represent channel widths. The curve is the least-squares fit to the data points of a thermal bremsstrahlung function with a best-fit temperature of 140 ± 12 keV. First and last energy channels have been excluded from the fit.

3.4. *Assessment of Uncertainties*

We have measured the spectrum of the Crab, the standard candle of X-ray astronomy, using a technique similar to that used for the Cygnus observations both to assess the systematic uncertainties in the fitted parameters and to evaluate the whole deconvolution procedure that we use to determine the photon flux spectra from the measured count rate distribution. The Crab lies within 1°.5 of the ecliptic plane, so it was in the normally solar-pointing FOV from mid-May through mid-July. The hard X-ray output of the Crab is constant corresponding to about 9 counts s^{-1} over the full HXRBS energy range in 1987. Thus, since the same techniques were used for both sources, we can use deviations in the Crab flux measure-

ments to estimate the uncertainties in the Cygnus flux measurements. In 1987 June and July, there were four Crab offpoints that were operationally similar to the Cygnus offpoints except that in three cases the Crab remained in the FOV (but at different angles to the collimator axis) during both the solar-pointing and offset-pointing periods. The standard deviation on the measured flux calculated for each individual fit using the linear regression method discussed by Bevington (1969) is close to the value calculated using Poisson statistics. For a typical offpoint of the Crab, the statistical uncertainty obtained from the fit is ~ 0.16 counts s^{-1} on the quantity $E \times$ FAREA over the entire energy range. This uncertainty compares with the 8–12 counts s^{-1} which we typically measured in $E \times$ FAREA during both the Crab and Cygnus observations. FAREA is taken as the maximum difference in FAREA for on-source versus off-source pointing exclusive of Earth occultation intervals; that is, $E \times$ FAREA is the increased count rate due to the source. From the four Crab offpoints, the deviation in E about the average value was found to be larger than this statistical uncertainty. We assume that this excess was due to an additional systematic error in determining $E \times$ FAREA of ~ 0.25 counts s^{-1} that adds in quadrature with the statistical uncertainty to yield the total uncertainty. The first 10 Cygnus offpoints, where we could not use the off-source background because of the Galactic center being in the FOV, were similar to fitting observations of the Crab for which there were only Earth occultations and no offpoint maneuvers. Analyzing the deviations about the average flux for several weeks of such occultations in May and June of 1987 shows that a systematic uncertainty of ~ 0.9 counts s^{-1} should be added in quadrature to the statistical uncertainty of ~ 0.4 counts s^{-1} on the quantity $E \times$ FAREA for a single occultation.

We have compared the Crab spectra obtained in this way with the spectrum reported by Strickman, Johnson, & Kurfess (1979) by iteratively fitting our spectra to a broken power-law spectrum, that is, two power laws which meet at a break energy. The power-law indices found were -1.7 ± 0.1 and -2.5 ± 0.1 below and above, respectively, a break at 76 ± 5 keV, compared to -2.0 and -2.4 reported by Strickman below and above a break at 80 keV for the steady state component and a single power law with an index -2.0 for the smaller pulsed emission. The flux integrated over the HXRBS broken power-law spectrum is greater by $3.5\% \pm 1.5\%$ than the flux reported by Strickman in the range from 45–140 keV, which is the range we use for comparison with the 20 yr synoptic results of Cygnus X-1 reported by Ling et al. (1987a). By varying the assumed gain used to deconvolve these Crab spectra and then comparing the results to the flux reported by Strickman, we have also estimated that for 1987 there is an uncertainty of $\pm 5\%$ in our knowledge of the detector gain for an on-axis source.

From the results described above and a related analysis of occultation measurements of the Crab flux in 1987 May, June, and July, we discovered a possible asymmetry in the detector response as a function of offset angles. These occultation analyses yielded differences in the source count rate which could be best explained by an effective gain, that is, the relation between pulse amplitude from the PMTs and the energy loss in the CsI(Na) crystal, which depended on the portion of the detector area illuminated by the source. The cause may have been due to a loss of optical coupling between one or more of the four PMTs and the CsI(Na) detector crystal. The effective gain apparently depended both on the angle away from the axis and the azimuth of the Crab as seen from the detector. (The Crab offpoint data used for the spectral comparison discussed above were corrected for this effect.) In addition to using the Crab occultation measurements to analyze the asymmetry, we have also studied the deviations in the fits to the flux from Cygnus X-1 during the pitch slews for each offpoint. Both of these data sets together suggest that, for measurements of sources at off-axis angles less than 25° along the azimuth of the Cygnus observations, the gain is equal to the on-axis gain within the 5% uncertainty in that value. Therefore, we have used the on-axis gain to analyze and deconvolve the measured count-rate spectra of Cygnus X-1.

4. RESULTS

Table 2 lists the best-fit free parameters to the source-plus-background model for each of the offpoints. The date and time of Table 1 are given as the Julian day in Table 2. These listed parameters have been summed over the 15 energy channels, and the corresponding uncertainties listed are those obtained from the fit and do not include the additional systematic uncertainties discussed above. The 45–140 keV flux values given in column (13) of Table 2 were determined by integrating a fit to the inverse-Compton (see § 4.2) photon spectrum over that energy range. The conversion factors used to convert the count rate spectrum to a photon spectrum were for a thermal bremmstrahlung spectrum with a temperature of 120 keV, close to the best-fit values that we obtain. The conversion factors vary slowly with temperature so that the uncertainties in the calculated flux introduced by the range of possible temperatures is less than a few percent. The uncertainty in the flux found in the last column of Table 2 is given as a fraction of the 45–140 keV flux and is taken to be the same as for the fractional uncertainty in the source count rate over the whole energy range which includes both the statistical component, σE, given in column (12) of Table 2, and the systematic component discussed previously in § 3.4. The uncertainty in the count rate measurement discussed in § 3.4 was for the entire detector energy range, $\sim$30–500 keV, but we have chosen to use the same fractional uncertainty for this smaller range of 45–140 keV because the bulk of the background rate and the Cygnus count rate flux lie within this energy range.

4.1. *Temporal Results*

The intensity of this 45–140 keV flux is plotted as a function of time in Figure 3 for each of the 30 observations. Most of the data lies close to or within a range bounded by the reported values for the γ_2 (0.13 photons cm^{-2} s^{-1}) and γ_3 (0.18 photons cm^{-2} s^{-1}) levels (Ling et al. 1987b) with the average flux for each year's observations represented by the solid lines. The average flux for observations 11 through 24 during the first year is 0.157 ± 0.005 photons cm^{-2} s^{-1} and for the second year is 0.136 ± 0.006 photons cm^{-2} s^{-1}. Thus, the second year flux is $\sim 3\ \sigma$ below the first year average where the uncertainty is due principally to variations in the source intensity during both epochs. The average flux of the first 10 observations is close to that of observations 10 through 24 even though the uncertainties are larger because the Galactic center region was in the FOV as discussed in § 3.2. Of the 14 observations made after 1987 February 1, the flux of 13 lie within a range of ± 0.02 photons cm^{-2} s^{-1} roughly centered about the full first year average flux of 0.154 ± 0.007 photons cm^{-2} s^{-1}. The six offpoints in 1988 also show a similar range of dispersion about

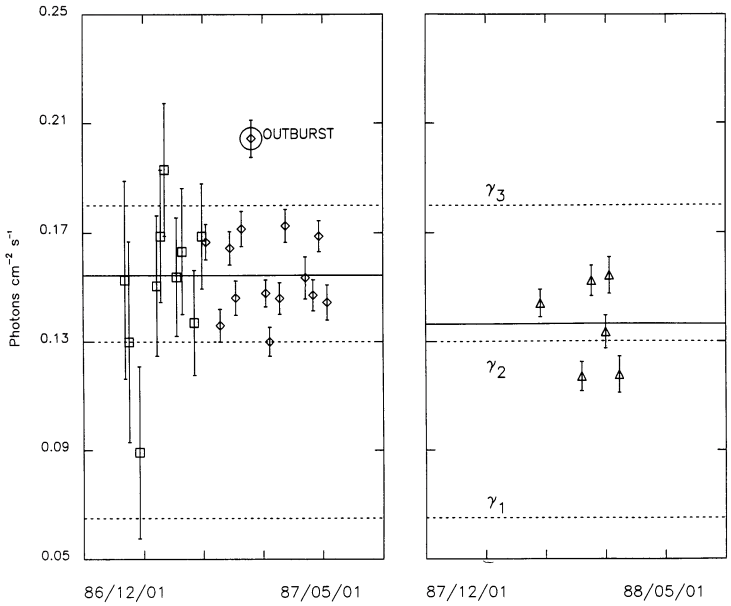

FIG. 3.—Cygnus X-1 light curve for the 45–140 keV band. Square data points are for the first 10 offpoints. These points have larger uncertainties because the Galactic center was in the FOV during solar pointing and only the offpoint data could be used. Diamonds, 1987, and triangles, 1988, represent the offpoint data with usable solar-pointing background. Error bars represent $\pm 1\ \sigma$ uncertainties calculated as the sum in quadrature of both the statistical and systematic uncertainties. Solid lines represent the averages of the measured fluxes in each of the two years, 0.154 photons cm^{-2} s^{-1} in 1986/1987 and 0.136 photons cm^{-2} s^{-1} in 1988. Reported fluxes of the γ_1, γ_2, and γ_3 levels (Ling et al. 1987a) are represented by the dashed lines. The outburst on 1987 February 24 is marked by the circled diamond above the γ_3 level.

their mean value. In both cases, the dispersion is ~ 2.0 times greater than would be expected for random deviations based on the measurement uncertainties.

We believe that the increased flux on 1987 February 24 shown in Figure 3 is a real outburst from the source. The 45–140 keV flux was 0.204 ± 0.007 photons cm^{-2} s^{-1}, a value at least 3 σ above the γ_3 level of 0.18 photons cm^{-2} s^{-1} and 7 σ above the average for 1987. The parametric fit to the count rate versus time for that day appears normal without any obvious distortions created by unusual magnetospheric events. We have looked at the possibility that the higher count rate could have been produced by an effect intrinsic to the detector. Because of the shape of the Cygnus X-1 count rate spectrum, the measured count rate in the HXRBS energy range of 30–500 keV would increase if there were an increase in the effective detector gain. To illustrate that much of the variability in our measurement of the source flux cannot be due to gain variations, the total Cygnus count rate is plotted versus the offpoint angle in Figure 4. Note that the outburst, marked with the circle overlaying the diamond, is at one of the larger off-axis angles, but that the count rate for an offpoint of comparable angle and uncertainty in the count rate lies almost 30% lower. Similarly, other pairs of offpoints show statistically significant differences in their count rates despite having small differences in off-axis angles.

We have not found evidence of intensity variations on shorter time scales ranging from our basic sample average of 16.384 s through 8 minutes after comparing histograms of the fit residuals during the on-source and off-source observing intervals. The distributions are Gaussian except for deviations seen for the longer sample times, which appear to have their origin in the simplifying assumptions made for the background model. Also, we have no evidence in the data for short-term deviations of the magnitude of the 1987 February 24 outburst. In 20 minutes a similar outburst would have been of order 6 σ above the average flux.

4.2. *Spectral Results*

Our spectral results are summarized in Figure 5, which shows both the outburst spectrum on 1987 February 24 and the spectrum obtained by taking an unweighted average over

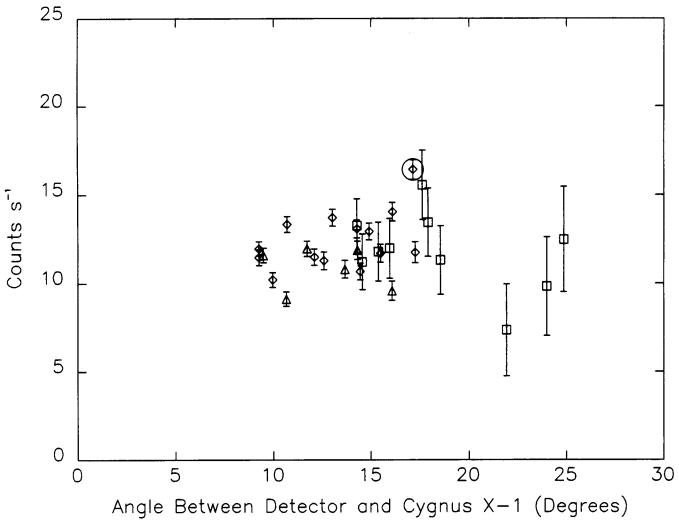

FIG. 4.—Total ($\sim$30–500 keV) count rate from Cygnus X-1 for all 30 observations as a function of the angle between the detector axis and the direction to the source. Symbols and error bars have the same significance as in Fig. 3. The outburst on 1987 February 24 is marked by the circled diamond.

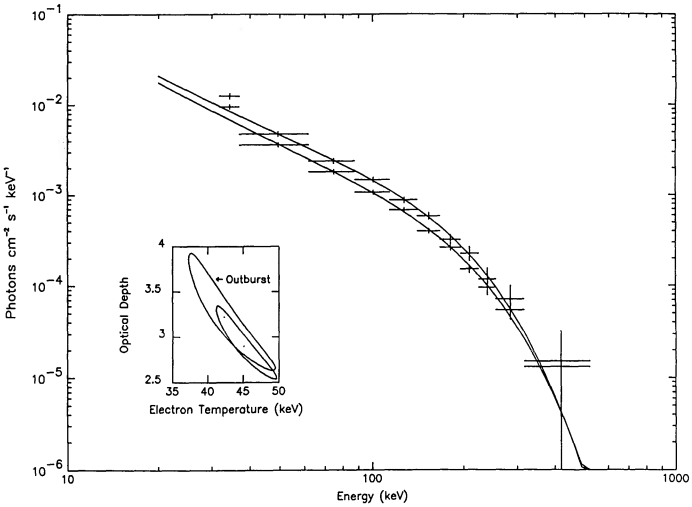

FIG. 5.—Measured spectrum (*upper points*) of Cygnus X-1 during the outburst on 1987 February 24 and the spectrum (*lower points*) averaged over the other observations from 1987 February 1 to 1987 April 3. The two highest energy data points in each case are averages over HXRBS energy channels 10–13 and 14–15, respectively. Error bars have the same meaning as those in Fig. 2. Curves are Comptonized thermal spectra (Sunyaev & Titarchuk 1980) fitted to each data set (excluding the first channel). Inset shows the 68% confidence contours ($\chi^2_{\min} + 2.3$) for the fit of the model to both spectra where the larger area represents the contour for the outburst spectrum. The best fit is indicated by the dot at the center of each contour area. At 100 keV, the average and the outburst fluxes are $1.07 \pm 0.03 \times 10^{-3}$ and $1.46 \pm 0.04 \times 10^{-3}$ photons cm^{-2} s^{-1} keV^{-1}, respectively.

the 13 other observations in the sequence 11 through 24 in Table 1. These two count rate spectra were deconvolved into photon spectra by the method described previously in § 3.4 using a thermal bremsstrahlung model function with a resultant temperature close to 120 keV. Using the photon spectra deconvolved in this way, the spectra shown in Figure 5 were obtained by making a least-squares fit to the inverse-Compton model of Sunyaev & Titarchuk (1980). This model gives the emergent Compton-scattered photon spectrum from a spherical, isothermal, hot, electron cloud of Thompson optical thickness τ in which a source of softer photons ($E \ll kT_e$) is embedded. (Although we did not use the conversion factors obtained from the inverse-Compton function to deconvolve the count rate spectrum, the difference in shape between this model and the thermal bremsstrahlung model is small enough over this energy range that the conversion factors used are accurate to within a few percent between 40 and 200 keV.) For the fit to the averaged spectrum, kT_e is 45 ± 4 keV and τ is 2.9 ± 0.3 while the fit parameters are 42 ± 6 keV and 3.2 ± 0.7 for the outburst spectrum. At 100 keV the fluxes are $(1.07 \pm 0.03) \times 10^{-3}$ and $(1.46 \pm 0.04) \times 10^{-3}$ photons cm^{-2} s^{-1} keV^{-1}, respectively. The uncertainties on kT_e and τ are taken from the extrema of the 68% confidence contours ($\chi^2_{\min} + 2.3$) which were determined by the method of Lampton, Margon, & Bowyer (1976). We have plotted these contours in the inset of Figure 5 for kT_e and τ with the normalization constant chosen so that χ^2 is minimized at each point in the grid. The overlap of the contours shows that the data are consistent with no change in spectral shape during the outburst. We have also fit the photon spectrum averaged over the 1988 observations and found that kT_e is 51 ± 7 keV, that τ is 2.6 ± 0.5, and that the flux at 100 keV is $(0.94 \pm 0.04) \times 10^{-3}$ photons cm^{-2} s^{-1} keV^{-1}. Thus, the average spectrum for the 1988 observations is also consistent with the shape of the spectrum measured during 1987, but with a drop in intensity of 12% near 100 keV.

The detector gain uncertainty of $\pm 5\%$ discussed in § 3.4 was not included in the calculation of the uncertainties of the spectral parameters given above. When comparing these values to those from other instruments, it is important to know how this uncertainty propagates to the derived spectral parameters. Specifically, if the detector gain were 5% higher than we have assumed, then the measured value of the 45–140 keV flux would be 3% lower, the value of the fitted flux at 100 keV would be 5% lower, the measured value of kT_e would be 8% lower, and the measured value of τ would be 3% higher than the values stated above.

5. DISCUSSION

In Figure 6 we present a summary of the results of our measurements of the hard X-ray spectrum of Cygnus X-1 along with the results of similar, extended spacecraft observations made with *HEAO 1* (Nolan & Matteson 1983) and with *HEAO 3* (Ling et al. 1983; Ling et al. 1987b). We present our data with increased uncertainties as discussed in the previous paragraph. The top row of Figure 6 shows the flux in the 45–140 keV band; the second and third rows show the best fits to the parameters of the Sunyaev-Titarchuk (1980) Comptonized thermal model. During all of these spacecraft observations the shape of the hard X-ray spectrum could be characterized by a temperature of ~40–55 keV and an optical depth parameter of ~2–3. Only the parameters of the fit to the γ_3 spectrum, where kT_e is 49 ± 4 keV and τ is 2.5 ± 0.25, fall well within the boundaries of the formal confidence region, shown in the inset to Figure 5, of the fit to the 1987 spectrum. Yet, considering the difficulties of comparing observations made with different detectors, there is no statistically significant difference in shape between all of these spectra over the energy range (~40–300 keV) of these observations.

There are, however, statistically significant differences in the fluxes although most of them fall close to, or between, the γ_2 and γ_3 levels. The 45–140 keV flux measured during the 1987 February 24 outburst was close to the intensity of Cygnus measured during an observation made with *HEAO 1*. Figure 1*c* of Nolan & Matteson (1983) shows a light curve of their observations made from 1978 October 14 through November 27 with the 45–140 keV flux from a single observation on 1978 November 1 at a level of 0.195 ± 0.004 photons cm^{-2} s^{-1}, that is, consistent with the 0.204 ± 0.007 photons cm^{-2} s^{-1} outburst flux measured with HXRBS. An observation approximately one day later showed that the flux had fallen back half-way to the average, and within two days the Cygnus flux was back close to the average shown in Figure 6*a*. In the 20 yr light curve of the Cygnus hard X-ray flux compiled by Ling et al. (1987a), the observation reported by Chodil et al. (1968) of a 45–140 keV flux of ~0.21 photons cm^{-2} s^{-1} was the only one to exceed 0.2 photons cm^{-2} s^{-1}. Examining the individual observations reported by Ling et al. (1983; 1987b) and Nolan & Matteson (1983), the hard X-ray flux normally fluctuates by $\sim \pm 10$–15% about a value which ranges from 0.12 to 0.18 photons cm^{-2} s^{-1}. There are brief outbursts on a time scale of hours to days where the intensity increases by ~30%, but the overall level appears to be stable on a time scale of months.

There was no evidence that the flux from Cygnus X-1 was as low as that from the γ_1 level during the HXRBS measurements.

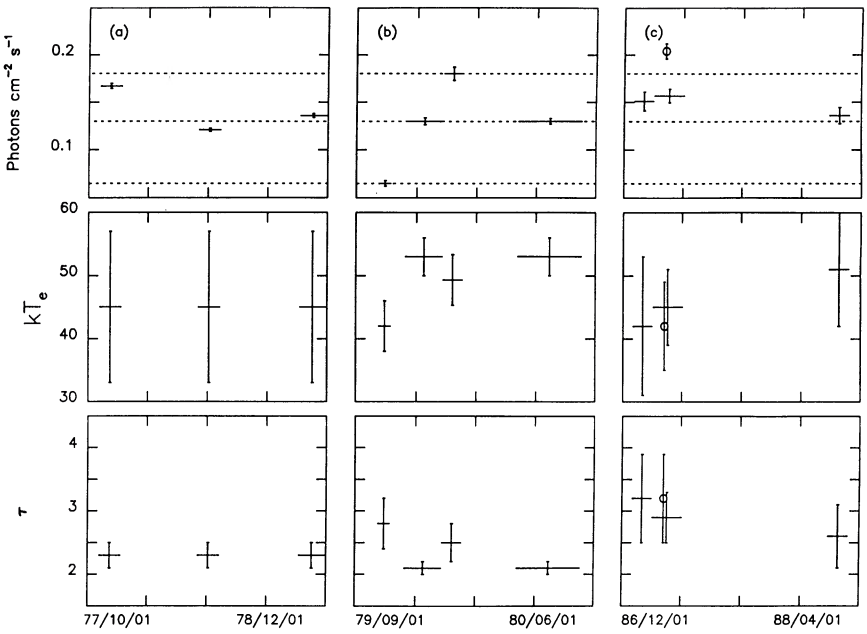

FIG. 6.—Best-fit parameters of the hard X-ray spectrum of Cygnus X-1 as measured with three spacecraft. Horizontal bars for each data point represent the period covered by a specific observation. The top row of plots shows the photon flux in the 45–140 keV band where the error bars represent $\pm 1\ \sigma$ uncertainties due to the intrinsic variability of the source. The γ_1, γ_2, and γ_3 levels are shown as in Fig. 3. The second and third row show the best-fit parameters to the Comptonized thermal model of Sunyaev & Titarchuk (1980) where kT_e and τ are the electron temperature and optical depth, respectively. Error bars represent the 1 σ uncertainties quoted by the respective authors. (*a*) Three epochs of observations made with *HEAO 1* as reported by Nolan & Matteson (1983). Spectral parameters were obtained from one component of a two-component fit in the 15–180 keV energy range. (*b*) Four epochs of the *HEAO 3* observations during which the Cygnus flux was at the γ_1, γ_2, γ_3, and γ_2 levels, respectively (Ling et al. 1983; Ling et al. 1987b). Spectra were fitted over the 50–300 keV range (50–400 keV for the γ spectrum). (*c*) HXRBS measurements where the outburst is again denoted by the circle. Uncertainties on the HXRBS measurements have been increased to reflect a $\pm 5\%$ uncertainty in the detector gain. (Note that the dates are for the start and end times of each of the three panels of plots.)

However, these measurements were taken over a period of several months with intervals as long as 10 days between observations. The *HEAO 3* measurements found the emission from Cygnus X-1 to be at the γ_1 level over a 2 week period with an additional 2 week period covering the transition to emission at the γ_2 level. Based on such a period of at least 1 month where the emission from Cygnus would be less than the γ_2 level, we believe that Cygnus X-1 was not emitting at the γ_1 level at any time during the two epochs of observation (see Table 1). Such emission may occur over shorter intervals, but it would require more frequent observations to detect it. Ling et al. (1987a) claim that other observations showing Cygnus X-1 with the low soft X-ray flux, low hard X-ray flux, and gamma-ray flux which are all characteristic of the γ_1 level suggest that the time scale for recurrence may be of order of 2 yr.

A key to the understanding of the hard X-ray emission of Cygnus X-1 may come from contemporaneous observations of the X-ray and gamma-ray spectra. Both the "low" and "high" state transitions and the γ_1 level observation have shown that changes in the intensity in a high-energy band are usually accompanied by an anticorrelated change in a low-energy band (Holt et al. 1976; Dolan et al. 1979; Ling et al. 1983, 1987b; Ling & Wheaton 1989b). During the *increase* from a "low" to "high" soft X-ray state, the hard X-ray flux has been observed to *decrease* in intensity. The γ_1 level has been associated with a low X-ray flux in two bands, one below 10 keV and the other from 40–400 keV, and a striking MeV gamma-ray component equal in luminosity to the hard X-rays (Ling et al. 1987b). There is also marginal evidence of a narrow annihilation line at 511 keV from Cygnus X-1 at the time of the γ_1 level emission. According to models of the Cygnus X-1 system (Shapiro, Lightman, & Eardley 1976; Sunyaev & Titarchuk 1980; Liang & Dermer 1988), there may be several physical components, such as a positron-dominated inner cloud and a proton-dominated outer accretion disk, which reprocess photons from other regions. For example, in the model of Sunyaev & Titarchuk, soft photons are Compton scattered to higher energy by hotter electrons, and increased numbers of these soft photons could conceivably cool the high-energy electrons.

The evidence is inconclusive as to whether to expect another component of high-energy emission above the HXRBS energy range, that is, >500 keV. There was some evidence from *HEAO 3* for emission from 500–1000 keV during the time of the γ_2 level emission and none at all during the time of the γ_3 level emission (Ling et al. 1987b). Nolan & Matteson (1983) showed some evidence of enhanced emission from 500–1000 keV during the 1977 and 1978 observations made with *HEAO 1*.

During the period of the HXRBS observations of Cygnus X-1, there were other instruments capable of making measurements of the spectrum at low and high energy; the All-Sky-Monitor on the Japanese *Ginga* spacecraft was sensitive from 1–30 keV; and the Gamma Ray Spectrometer (GRS) on *SMM* was sensitive from 0.3–10 MeV. The data from the All Sky Monitor consists of 4–6 s scans of Cygnus X-1 through the FOV every few days during the period of the HXRBS observations while the analysis of the GRS data has been delayed by the effort required to reduce the systematic uncertainties (Ling 1990, private communication). There was a series of observa-

tions of Cygnus X-1 from 30–180 keV made with the High Energy X-ray Experiment (HEXE) on the Soviet space station *Mir* from 1987 July 18 through 1989 April 25 (Döbereiner et al. 1989). They found that during observations prior to and immediately after the HXRBS observations in 1988 that the value of the fitted flux at 100 keV was $(0.80 \pm 0.01) \times 10^{-3}$ photons cm^{-2} s^{-1} keV^{-1}, the value of kT_e was 37.4 ± 1 keV, and the value of τ was 3.8 ± 0.1. Shortly thereafter in two observations on 1988 May 8–9 the flux was found to have increased threefold while the spectral parameters remained consistent with no change. The difference between the flux at 100 keV measured with HEXE and that measured with HXRBS is small enough to suggest that there was no difference in the emission level of Cygnus X-1 from 1987 July 18 until 1988 April 28. It will require analysis of the spectrum and time variability of the flux of Cygnus X-1 over the energy range covered by the data from all of these instruments to place our measurements in context relative to measurements from previous epochs.

There are similarities in temporal and spectral variations which have been attributed to both Cygnus X-1 and a hard X-ray/gamma-ray source believed to lie close to the Galactic center (Lingenfelter & Ramaty 1989; Ling & Wheaton 1989a, b). After subtracting away the annihilation line radiation associated with a diffuse steady source, the Galactic center source spectrum above 500 keV is in good agreement with that of the γ_1 level. Thus, Lingenfelter & Ramaty have speculated that, like Cygnus X-1, the Galactic center source is also a stellar-size black hole. However, despite numerous observations of both sources, the only definitive measurements of Cygnus X-1 and the Galactic center with this type of spectroscopy were made with *HEAO 3* over separate 2 week intervals in late 1979 (see Lingenfelter & Ramaty 1989; Ling & Wheaton 1987a, b). The observation of the γ_1 level of Cygnus X-1 shows, when compared to the more normal γ_2 spectrum, that the hard X-ray spectrum becomes less intense but flatter while a component around 1 MeV is present (Ling et al. 1987b); the equivalent of the γ_2 spectrum has not been defined for the Galactic center source because of the ambiguity of the wide field observations (Lingenfelter & Ramaty 1989).

It has been difficult to uniquely associate the Galactic center hard X-ray spectrum with the presumed source of the annihilation radiation due to the scarcity of line-emission measurements and the source confusion inherent with nonimaging detectors in the hard X-ray range. Since the Galactic center is only six degrees away from the ecliptic plane, this region passed through the HXRBS FOV in December and January of every year from 1980 December through 1989 January. Using the techniques described in this paper, it may be possible to determine the hard X-ray spectral shape and intensity of sources in this region for these time intervals. Given that the normal spectrum may be similar in shape to that of Cygnus X-1, the next step would be to examine whether there are γ_1-like levels in intensity. Taken together with the measurements made with *SMM*/GRS of the annihilation line flux (Share et al. 1988) and gamma-ray flux, as well as the upcoming measurements expected to be made with the Gamma Ray Observatory of the Galactic center and Cygnus X-1, a more complete picture of the physical processes in stellar-size black hole systems could be revealed.

The authors would like to express thanks to the *SMM* project for their operational and financial support. We give special thanks to James Barcus, Judith Nelson, Robert Shindock, Chris St. Cyr, David Kendig, Greg Slater, and Elaine Einfalt for operational support during the offpoints. R. S. expresses his appreciation of the efforts of Francesca Crannell, Tomas Koshut, and Teresa McCloud for helping to assemble the data base. We thank A. Kimberley Tolbert for ongoing software support. J. C. L. and W. A. W. participated in this research as *SMM* guest investigators. The research of J. C. L. and W. A. W. described in this paper was carried out by the Jet Propulsion Laboratory, California Institute of Technology, under contract with the National Aeronautics and Space Administration. R. A. S. was supported under contracts NAS-5-28572 and NAS-5-30440.

REFERENCES

Batchelor, D. A. 1984, Ph.D. thesis, University of North Carolina, Chapel Hill
Bevington, P. R. 1969, Data Reduction and Error Analysis for the Physical Sciences (New York: McGraw-Hill), 204
Chodil G., Mark, H., Rodrigues, R., & Swift, C. D. 1968, ApJ, 151, L1
Coe, M. J., Engel, A. R., & Quenby, J. J. 1976, Nature, 259, 544
Döbereiner, S., et al. 1989, Proc. 23rd ESLAB Symp. on Two-Topics in X-Ray Astronomy (Bologna: ESA SP-296), 387
Dolan, J. F., Crannell, C. J., Dennis, B. R., Frost, K. J., & Orwig, L. E. 1977, Nature, 267, 813
———. 1979, ApJ, 230, 551
Holt, S. S., Boldt, E. A., Serlemitsos, P. J., & Kaluzienski, L. J. 1976, ApJ, 203, L63
Lampton, M., Margon, B., & Bowyer, S. 1976, ApJ, 208, 177
Levine, A. M., et al. 1984, ApJS, 54, 581
Liang, E. P., & Dermer, C. D. 1988, ApJ, 325, L39
Ling, J. C., Mahoney, W. A., Wheaton, Wm. A., & Jacobson, A. S. 1987a, Proc. 20th Internat. Cosmic Ray Conf. (Moscow)
———. 1987b, ApJ, 321, L117
Ling, J. C., Mahoney, W. A., Wheaton, Wm. A., Jacobson, A. S., & Kaluzienski, L. 1983, ApJ, 275, 307
Ling, J. C., & Wheaton, Wm. A. 1989a, ApJ, 343, L57
Ling, J. C., & Wheaton, Wm. A. 1989b, Proc. Gamma-Ray Observatory Science Workshop, ed. Neil Johnson (Greenbelt, MD: Goddard Space Flight Center), 4-282
Lingenfelter, R. E., & Ramaty, R. 1989, ApJ, 343, 686
Matteson, J. L., Mushotzky, R. F., Paciesas, W. S., & Laros, J. G. 1976, Workshop Papers on X-ray Binaries (NASA SP-389) (Greenbelt, MD: Goddard Space Flight Center)
Ninkov, Z., Walker, G. A. H., & Yang, S. 1987, ApJ, 321, 425
Nolan, P. L., & Matteson, J. L. 1983, ApJ, 265, 389
Oda, M. 1980a, IAU Circ., No. 3402
———. 1980b, IAU Circ., No. 3491
Ogawara, Y., Mitsuda, F., Masai, K., Vallerga, J. V. Cominsky, L. R., Grunsfeld, J. M., Kruper, J. S., & Ricker, G. R. 1982, Nature, 295, 675
Orwig, L. E., Frost, K. J., & Dennis, B. R. 1980, Solar Phys., 65, 25
Share, G. H., Kinzer, R. L., Kurfess, J. D., Messina, D. C., Purcell, W. R., Chupp, E. L., Forrest, D. J., & Reppin, C. 1988, ApJ, 326, 717
Shapiro, S. L., Lightman, A. P., & Eardley, D. M. 1976, ApJ, 204, 187
Strickman, M. S., Johnson, W. N., & Kurfess, J. D. 1979, ApJ, 230, L15
Sunyaev, R. A., & Titarchuk, L. G. 1980, A&A, 86, 121
Tananbaum, H., Gursky, H., Kellogg, E., & Giacconi, R. 1972, ApJ, 177, L4
Wheaton, Wm. A., Dunklee, A. L., Jacobson, A. S., Ling, J. C., Mahoney, W. A., & Radocinski, R. G. 1990, ApJ, submitted